Bacterial filamentation is an in vivo mechanism for cell-to-cell spreading

Short title: Cell-to-cell spreading via filamentation

One sentence summary: An intracellular bacterial pathogen uses filamentation to invade neighboring host intestinal cells

Tuan D Tran[1], Munira Aman Ali[1], Davin Lee[1], Marie-Anne Félix[2], Robert J Luallen[1*]

[1]Department of Biology, San Diego State University, San Diego, CA 92182, USA

[2]Institut de Biologie de l' École Normale Supérieure, Centre National de la Recherche Scientifique, INSERM, École Normale Supérieure, Paris Sciences et Lettres, Paris, France

[*]Corresponding author. Email: rluallen@sdsu.edu

Abstract
Intracellular pathogens are challenged with limited space and resources while replicating in a single host cell. Mechanisms for direct invasion of neighboring host cells have been discovered in cell culture, but we lack an understanding of how bacteria directly spread from cell-to-cell in vivo. We have discovered a bacterial species that uses filamentation as an in vivo mechanism for intracellular spreading between the intestinal epithelial cells of its host, the rhabditid nematode *Oscheius tipulae*. In vitro and in vivo filamentation by this bacterium, *Bordetella atropi*, requires a conserved nutrient-sensing pathway used by divergent bacteria to detect rich conditions and inhibit the divisome. Thus, *B. atropi* uses a novel mechanism for cell-to-cell spreading by coopting a pathway that regulates bacterial cell size to trigger filamentation inside host cells.

Main Text

Pathogenic invasion of host cells often provides microbes with a major benefit, including a high concentration of metabolic resources and protection from extracellular immunity (*1*). An individual host cell, however, represents a small niche and intracellular pathogens must spread to other cells in order to maximize the use of host resources. All intracellular microbes can spread via extracellular escape from the initial infected cell, a process that leaves them vulnerable to host defenses. Some microbes, however, have evolved unique mechanisms to invade uninfected host cells directly from an initial infected cell. To date, two main paradigms for cell-to-cell spreading by bacteria have been described, both of which converge on effector-driven manipulation of host actin. In one mechanism, *Listeria monocytogenes*, *Shigella flexneri*, and *Rickettsia spp.* can polymerize host actin for cytoplasmic propulsion of bacteria into the lateral membrane for uptake by neighboring cells (*2*). *Burkholderia* spp. also use actin-based propulsion, but invasion of neighboring cells is facilitated by fusion of the lateral membranes (*3*). In another mechanism, *Ehrlichia chaffeensis* can directly transfer from a phagocytic cell to a target cell through actin-dependent filopodia formation, although it is unclear if this mechanism is directly initiated by the pathogen (*1*, *4*). Each of these bacterial mechanisms has only been directly observed in cell culture systems, bringing up the possibility of alternative mechanisms for cell-to-cell spreading and dissemination in vivo (*5*).

Bacteria often change their cell shape as a fitness strategy to survive or thrive in diverse environments. Filamentation is one form of morphological plasticity, often used as a survival strategy in toxic or stressful environments. During filamentation, there is a dramatic increase in cell length as a bacterium divides longitudinally multiple times without daughter cell separation, often without septation (*6*, *7*). Gram-negative bacteria are mainly known to undergo filamentation after exposure to environmental stressors, including DNA damage and β-lactam antibiotics, which induce the SOS response (*6*). Several bacterial pathogens have been observed to filament in vivo, including inside host cells (*8*). However, to our knowledge, filamentation has never been observed to be used for cell-to-cell spreading by any intracellular pathogen, including bacteria or fungi (*9*).

We discovered the first intracellular bacterial pathogen of free-living nematodes. From ecological sampling, we isolated a wild *Oscheius tipulae* strain (JU1501) from rotting crab apples (Fig. S1). *O. tipulae* is a rhabditid species that is commonly found in soil and decomposing vegetation. In JU1501, coccobacilli-shaped microbes were observed to infect the intestinal epithelial cells (Fig. 1A) (*10*). This microbe was originally reported in a survey of microsporidian parasites based on morphology, however, microsporidian-specific 18S primers failed to produce an amplicon (*11*). Here, we conducted fluorescence in situ hybridization (FISH) on mixed populations of this *O. tipulae* strain and found that microsporidian-specific 18S probes failed to bind (Fig. S2A), while a universal probe to bacterial 16S rRNA showed strong hybridization with thousands of coccobacilli inside the animal (Fig. 1B). Additionally, a second bacterial morphology was observed in some animals using the same FISH probe in which long filaments extended

throughout the intestine (Fig. 1C). Identical phenotypes were seen using a FISH probe specific to the 16S rRNA of this bacterium but not a non-specific bacterial 16S probe (Fig. S2B-C).

We isolated this bacterium on LB agar plates (strain name LUAb4) and verified that it could reinfect JU1501 *O. tipulae* animals that were sterilized of all horizontally-transmitted microbes using a bleach treatment (as seen Fig. 1E-J). We sequenced the genome of LUAb4 and conducted phylogenomic analysis to find that the bacterium represents a new species in a separate monophyletic clade of *Bordetella* (Fig. 1D), clustering with Bordetellae isolated from human respiratory specimens or the environment. We named this bacterium *Bordetella atropi*, after Atropos, the Greek Fate who cuts the thread of life (Supp. Text 1, Taxonomic Summary).

Infection by *B. atropi* has a severe effect on host fitness with an approximate 2.5-fold decrease in average lifespan and 90-fold decrease in fecundity (Fig. 1E-F). We only observed *B. atropi* intracellular infection in intestinal cells. To verify this, we infected live animals with RFP-expressing *B. atropi* and fed them Cell Tracker Blue to stain the intestine. *B. atropi* filaments were only observed in intestinal epithelial cells (Fig. S3A). Similarly, analysis of Z-stacks from confocal images of fixed animals found that *B. atropi* intracellular phenotypes were only in the intestine, adjacent to DAPI-stained intestinal nuclei (Fig. S3B). We do commonly see *B. atropi* coccobacilli in the lumen of the pharynx and intestine, suggesting a fecal-oral route of infection. To determine the order of appearance of *B. atropi* phenotypes in vivo, we conducted a pulse-chase infection experiment and found that the majority of animals had short or long intracellular filaments at 16 and 24 hours post infection (hpi), while the majority of animal intestines were filled with coccobacilli at 36 and 48 hpi (Fig. 1G).

To more closely examine *B. atropi* infection phenotypes, we conducted transmission electron microscopy (TEM) of infected animals. *B. atropi* coccobacilli and filaments were distinguished from host cellular structures by their cell wall, which appears as a wavy, electron dense line surrounding a large nucleoid, similar to TEM images of intracellular *Bordetella bronchiseptica* (*12*). At 24 hpi, we can see filaments in intestinal cells that are unseptated with regularly spaced nucleoids and coccobacilli in the intestinal lumen (Fig. 1H). TEM only captures a portion of a filament length due to thin sectioning and the longest filament captured with this method was 10.06 μm (Fig. S4A). At 48 hpi, we see intestinal cells that are heavily infected with individual coccobacilli cells (Fig. 1I). Using quantification, we found that 42% of images displayed intestinal filaments at 24 hpi (n=52), and only 6.5% at 48 hpi (n=31), showing a similar trend to the emergence of phenotypes in vivo via fluorescence microscopy (see Fig. 1G). Separately, TEM bolstered the intestinal tropism seen with *B. atropi* as 70.6% of images had intracellular intestinal infection (n=102), but no infection was seen in non-intestinal tissues, including the muscle (n=38) and epidermis (n=73). The lateral intestinal membranes appear disrupted in infected animals as they are often missing or at oblique angles relative to the intestinal lumen in infected cells. This is in contrast to uninfected cells where they are relatively perpendicular to the lumen (Fig. S4B-C). Together, these observations

show that *B. atropi* is an intracellular pathogen that first filaments in intestinal epithelial cells and later septates into individual coccobacilli before exiting the host cell.

We hypothesized that filamentation is used as a mechanism for cell-to-cell spreading. Often, we observed cases where filaments passed near multiple intestinal nuclei, indicating that the bacterium was simultaneously infecting neighboring intestinal cells (Fig. 2A). To test this hypothesis, we sought to isolate a non-filamenting mutant of *B. atropi*. Similar to *Bordetella avium* (*13*), our bacterium could be induced to filament in vitro by switching growth from Luria broth (LB) to the richer medium Terrific broth (TB) (Fig. S5A), allowing us to use in vitro selection to isolate filamentation mutants (Fig. 2B). We focused on one mutant, LUAb7, which formed less frequent and much shorter filaments in vitro compared to wild type (Fig. 2C), but grew at the same rate (Fig. 2D). In vivo infection of *O. tipulae* found that LUAb7 also failed to form long filaments and showed significantly decreased anterior-posterior spreading (Fig. S5B-C). The intestine of *O. tipulae* consists of left-right pairs of polarized epithelial cells running along the anterior-posterior (A-P) axis (*14*). To quantify the cell-to-cell spreading capacity of WT and LUAb7, we pulse infected animals for a short period to limit the number of invasion events and then counted the number of intestinal nuclei that each contiguous infection event passes along the A-P axis. Single WT *B. atropi* filaments spanned an average of 5.7 and a maximum of 15 intestinal nuclei (Fig. 2E-F). By contrast, LUAb7 failed to consistently form filaments in vivo, with replicating infection foci seen spanning an average of 1.9 and a maximum of 4 intestinal nuclei. Similar to *C. elegans,* intestinal nuclei in *O. tipulae* may undergo one nuclear division without cell division during development. Using intestinal membrane staining, we quantified an average of 1.9 intestinal nuclei per cell at both the anterior and posterior end (Fig. S6). Therefore, WT *B. atropi* filaments spread laterally to an average of 3 cells and a maximum of 8 cells at 32 hpi, while the filamentation mutant remains largely restricted to a single cell but occasionally spreads to another cell. Altogether, these data indicate that *B. atropi* uses filamentation as an intracellular mechanism for cell-to-cell spreading.

We identified the causative mutation in LUAb7 through whole genome sequencing and single nucleotide variations (SNVs) calling. The best candidate was a missense mutation found in *gtaB*, a UTP--glucose-1-phosphate uridylyltransferase. The mutation in *gtaB* lead to an R17C change in a predicted catalytic arginine found in a highly conserved N-terminal motif (Fig. 3A) (*15*). We complemented LUAb7 with $gtaB^{+}$ from *B. atropi* and found a rescue of in vitro filamentation (Fig. 3B) as well as in vivo filamentation, with similar levels of cell-to-cell spreading as wild type (Fig. 2E-F). Additionally, deletion of *gtaB* from WT *B. atropi* resulted in a loss of filamentation in vitro, similar to $gtaB^{R17C}$ (Fig. 3D). Thus, $gtaB^{R17C}$ is the causative allele for loss of filamentation in LUAb7 and this single mutation abolishes cell-to-cell spreading of the pathogen.

GtaB (GalU in *E. coli*) catalyzes the conversion of glucose-1-phosphate to UDP-glucose, a substrate in the production of cell wall components like osmoregulated periplasmic glucans (OPGs), lipopolysaccharide, and capsular polysaccharides (Fig. 3C). In *E. coli* and *Bacillus subtilis*, this UDP-glucose biosynthetic pathway serves as a

metabolic sensor that links carbon availability to growth rate (*16*). Excess UDP-glucose acts as a readout for rich conditions and temporarily inhibits FtsZ ring formation during replication for moderately larger progeny cells (*17*, *18*). In *E. coli,* FtsZ ring inhibition is mediated by OpgH, a downstream glucosyltransferase that is thought to sequester FtsZ monomers at the nascent division site in a UDP-glucose-dependent manner (Fig. 3C) (*17*). We tested other members in this pathway for a role in filamentation by knocking them out in *B. atropi*. Deletion of *opgH* resulted in a loss of filamentation in vitro, similar to LUAb7(*gtaB*^{R17C}) (Fig. 3D). The *B. atropi* genomes included two copies of phosphoglucomutase (pgm) and deletion of *pgm2* but not *pgm1* resulted in an in vitro filamentation phenotype (Fig. 3D). We tested these knockouts in vivo and found that the *opgH* knockout phenocopied LUAb7(*gtaB*^{R17C}), with reduced A-P spreading in the intestine (Fig. 3E). The *pgm1* knockout showed no change in spreading in vivo compared to WT, consistent with in vitro data. The *pgm2* and *gtaB* knockouts were attenuated in vivo, as we saw no intracellular infection with these strains despite populations of >500 animals per replicate (Fig. S7). In fact, we saw little to no bacteria in the intestinal lumen with these knockouts, suggesting that a complete loss of some cell wall components may result in an inability to survive feeding by *O. tipulae*, perhaps leaving bacteria sensitive to the posterior grinder and/or destruction by extracellular defenses in the lumen. Altogether, these results support a requirement for the UDP-glucose biosynthetic pathway and *opgH* in inhibiting cell fission in *B. atropi*, but in a more extreme manner than seen in *E. coli* and *B. subtilis,* leading to long multinucleoid filaments rather than bacilli with modestly increased lengths. Overall, we propose a model where *B. atropi* detects the nutrient-rich intracellular environment of an intestinal cell through the UDP-glucose biosynthetic pathway and OpgH in order to initiate filamentation for cell-to-cell spreading (Fig. 3F).

Together, our findings describe bacterial filamentation as an in vivo mechanism for cell-to-cell spreading in a host epithelium. Several human-infecting bacterial pathogens have been observed to filament in vivo, including some that filament intracellularly, bringing up the possibility that some pathogens may use filamentation as a spreading mechanism (*7*, *8*). Uropathogenic *E. coli* (UPEC) can form extremely long filaments inside umbrella cells, with conflicting data on whether these filaments are refractory to phagocytosis by macrophages after their release from host cells (*19*, *20*). Intracellular bacterial filaments can distort host cell shape in cell culture, as *Yersinia pestis* filaments in macrophages can make protrusions in the host cell membrane (*21*) and *Salmonella typhimurium* filaments can grossly distort and elongate primary melanocytes (*22*). It is possible that exaggerated longitudinal growth is an in vivo strategy that intracellular pathogens can use to push through the lateral membranes in an epithelial layer for invasion of neighboring cells. For example, microsporidian parasites in *C. elegans* can form elongated intracellular stages (called meronts) that distort lateral intestinal membranes, leading to the formation of a syncytial tissue and cell-cell spreading (*23*).

We found that filamentation induction by *B. atropi* is linked to the nutrient availability through a highly conserved metabolic pathway that inhibits the bacterial divisome under rich conditions. These findings represent a new mechanism for the induction of filamentation in bacteria that is independent of the SOS response. Given the broad

conservation of the UDP-glucose pathway and its role in delaying binary division on rich media (*17*, *18*), it is possible that the evolutionary steps for coopting this pathway for filamentation are minimal. For example, experimental overexpression of *opgH* in *E. coli* is sufficient to lead to filamentation, showing that altering the expression of a single gene in the pathway can induce this phenotype (*17*). *B. avium* is a respiratory pathogen of turkeys and was found to form filaments in TB similar to *B. atropi*, bringing up the possibility that filamentation in rich conditions is conserved among other clinically-relevant Bordetellae (*13*).

References

1. P. M. Colonne, C. G. Winchell, D. E. Voth, Hijacking host cell highways: Manipulation of the host actin cytoskeleton by obligate intracellular bacterial pathogens. *Front. Cell. Infect. Microbiol.* **6**, 1–8 (2016).
2. E. Weddle, H. Agaisse, Principles of intracellular bacterial pathogen spread from cell to cell. *PLoS Pathog.* **14**, e1007380 (2018).
3. W. Kespichayawattana, S. Rattanachetkul, T. Wanun, P. Utaisincharoen, S. Sirisinha, *Burkholderia pseudomallei* induces cell fusion and actin-associated membrane protrusion: A possible mechanism for cell-to-cell spreading. *Infect. Immun.* **68**, 5377–5384 (2000).
4. P. S. Dunphy, T. Luo, J. W. McBride, *Ehrlichia* moonlighting effectors and interkingdom interactions with the mononuclear phagocyte. *Microbes Infect.* **15**, 1005–1016 (2013).
5. G. Nikitas, C. Deschamps, O. Disson, T. Niault, P. Cossart, M. Lecuit, Transcytosis of *Listeria monocytogenes* across the intestinal barrier upon specific targeting of goblet cell accessible E-cadherin. *J. Exp. Med.* **208**, 2263–2277 (2011).
6. S. S. Justice, D. A. Hunstad, L. Cegelski, S. J. Hultgren, Morphological plasticity as a bacterial survival trategy. *Nat. Rev. Microbiol.* **6**, 162–8 (2008).
7. D. Yang, K. Blair, N. Salama, Staying in Shape: the Impact of Cell Shape on Bacterial Survival in Diverse Environments. *Microbiol. Mol. Biol. Rev.* **80**, 187–203 (2016).
8. E. Frirdich, E. C. Gaynor, Peptidoglycan hydrolases, bacterial shape, and pathogenesis. *Curr. Opin. Microbiol.* **16**, 767–778 (2013).
9. F. Dalle, B. Wächtler, C. L'Ollivier, G. Holland, N. Bannert, D. Wilson, C. Labruère, A. Bonnin, B. Hube, Cellular interactions of *Candida albicans* with human oral epithelial cells and enterocytes. *Cell. Microbiol.* **12**, 248–271 (2010).
10. D. Baïlle, A. Barrière, M. A. Félix, *Oscheius tipulae*, a widespread hermaphroditic soil nematode, displays a higher genetic diversity and geographical structure than *Caenorhabditis elegans*. *Mol. Ecol.* **17**, 1523–1534 (2008).
11. G. Zhang, M. Sachse, M.-C. Prevost, R. J. Luallen, E. R. Troemel, M.-A. Félix, A Large Collection of Novel Nematode-Infecting Microsporidia and Their Diverse Interactions with Caenorhabditis elegans and Other Related Nematodes. *PLoS Pathog.* **12**, e1006093 (2016).
12. D. L. Taylor-Mulneix, L. Bendor, B. Linz, I. Rivera, V. E. Ryman, K. K. Dewan, S.

M. Wagner, E. F. Wilson, L. J. Hilburger, L. E. Cuff, C. M. West, E. T. Harvill, *Bordetella bronchiseptica* exploits the complex life cycle of *Dictyostelium discoideum* as an amplifying transmission vector. *PLoS Biol.* **15**, 1–28 (2017).
13. D. T. Domingo, M. W. Jackwood, T. P. Brown, D. T. Domingo, A. M. W. Jackwood, T. P. Brown, Filamentous Forms of *Bordetella avium*: Culture Conditions and Pathogenicity. *Avian Dis.* **36**, 707–713 (1992).
14. M. L. Dichtel, S. Louvet-Vallée, M. E. Viney, M. A. Félix, P. W. Sternberg, Control of vulval cell division number ha the nematode *Oscheius/Dolichorhabditis* sp. CEW1. *Genetics*. **157**, 183–197 (2001).
15. M. Berbis, J. Sanchez-Puelles, F. Canada, J. Jimenez-Barbero, Structure and Function of Prokaryotic UDP-Glucose Pyrophosphorylase, A Drug Target Candidate. *Curr. Med. Chem.* **22**, 1687–1697 (2015).
16. J. D. Wang, P. A. Levin, Metabolism, cell growth and the bacterial cell cycle. *Nat. Rev. Microbiol.* **7**, 822–827 (2009).
17. N. S. Hill, P. J. Buske, Y. Shi, P. A. Levin, A Moonlighting Enzyme Links *Escherichia coli* Cell Size with Central Metabolism. *PLoS Genet.* **9**, e1003663 (2013).
18. R. B. Weart, A. H. Lee, A. C. Chien, D. P. Haeusser, N. S. Hill, P. A. Levin, A Metabolic Sensor Governing Cell Size in Bacteria. *Cell*. **130**, 335–347 (2007).
19. D. A. Rosen, T. M. Hooton, W. E. Stamm, P. A. Humphrey, S. J. Hultgren, Detection of Intracellular Bacterial Communities in Human Urinary Tract Infection. *PLoS Med.* **4**, e329 (2007).
20. S. S. Justice, D. A. Hunstad, P. C. Seed, S. J. Hultgren, Filamentation by *Escherichia coli* subverts innate defenses during urinary tract infection. *PNAS*. **103**, 19884–19889 (2006).
21. D. Ponnusamy, K. D. Clinkenbeard, *Yersinia pestis* intracellular parasitism of macrophages from hosts exhibiting high and low severity of plague. *PLoS One*. **7**, e42211 (2012).
22. M. J. Martínez-Lorenzo, S. Méresse, C. De Chastellier, J. P. Gorvel, Unusual intracellular trafficking of *Salmonella typhimurium* in human melanoma cells. *Cell. Microbiol.* **3**, 407–416 (2001).
23. K. M. Balla, R. J. Luallen, M. A. Bakowski, E. R. Troemel, Cell-to-cell spread of microsporidia causes Caenorhabditis elegans organs to form syncytia. *Nat. Microbiol.* **1** (2016), doi:10.1038/nmicrobiol.2016.144.

Acknowledgements
We would like to thank Prof. Aharon Oren for his expertise in prokaryotic nomenclature and assistance in naming *B. atropi*. Thank you to Dalaena Rivera for helping come up with the name *B. atropi*. We would like to thank Dr. Anca Segall and Dr. Nick Shikuma for providing bacterial plasmids, access to equipment, and assistance with bacterial genetics. Thank you to Dr. Aaron Reinke for editing the manuscript.

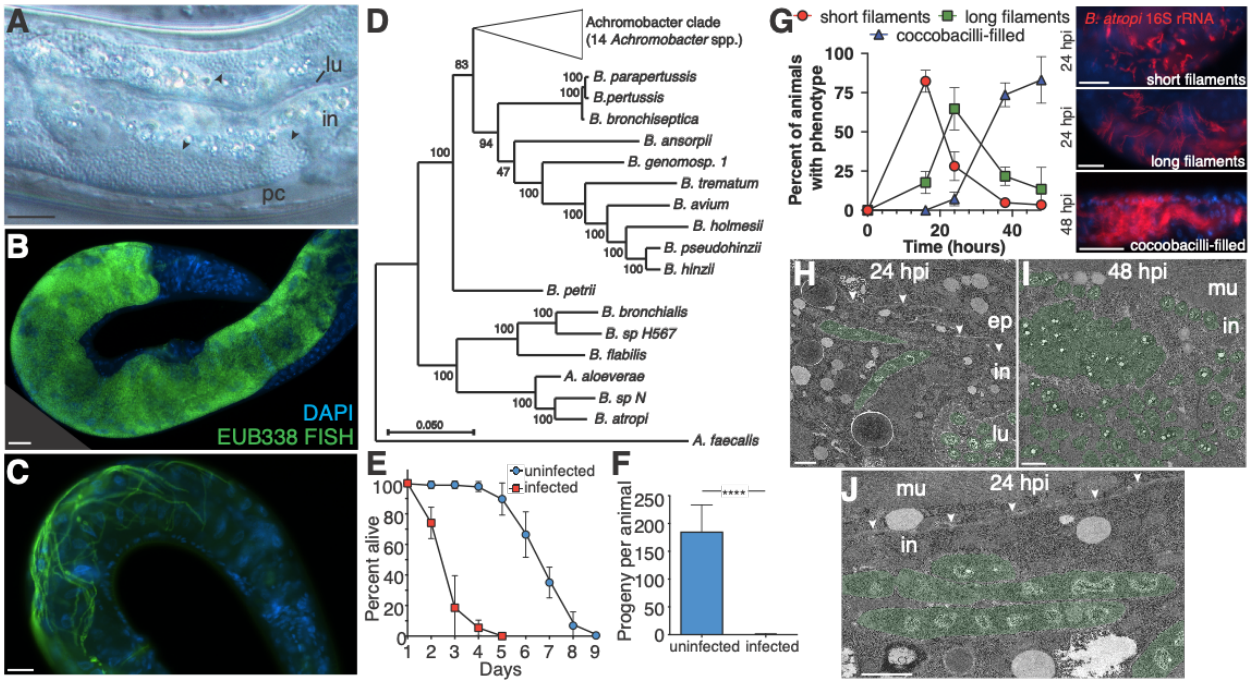

Fig. 1. *B. atropi* filaments in intestinal cells. (**A**) Clusters of coccobacilli (*arrowheads*) inside the intestinal cells (*in*) of *O. tipulae* strain JU1501. The intestinal lumen (*lu*) and pseudocoelom (*pc*) are indicated. (**B-C**) FISH using a universal bacterial 16S rRNA probe EU338. Different animals shown from the same plate. Scale bars are 20 μm. (**D**) Phylogenomic tree of sequenced *Bordetella* and *Achromobacter* spp. with outgroup *Alcaligenes faecalis*. Branch lengths are the number of substitutions per site and branch points indicate percentage of trees with clustering of associated taxa. (**E**) Lifespan of JU1501 infected or uninfected with *B. atropi*, n=20 animals in 3 independent replicates (**F**) Broodsizes of JU1501, **** is $p<0.0001$ by unpaired t test with Welch's correction, n=20 animals in 2 independent replicates. (**G**) Pulse chase infection time course with the mean and SD of two independent replicates shown. Representative infection phenotypes are shown. Scale bars are 20 μm. (**H-J**) TEM of *B. atropi* infected JU1501. Filaments at 24 hpi (H,J) and a cluster of coccobacilli at 48 hpi (I) are pseudocolored green. The intestine (*in*), muscle (*mu*), epidermis (*ep*), and intestinal lumen (*lu*) are indicated and the pseudocoelom is delineated (*arrowheads*). Scalebars are 1 μm.

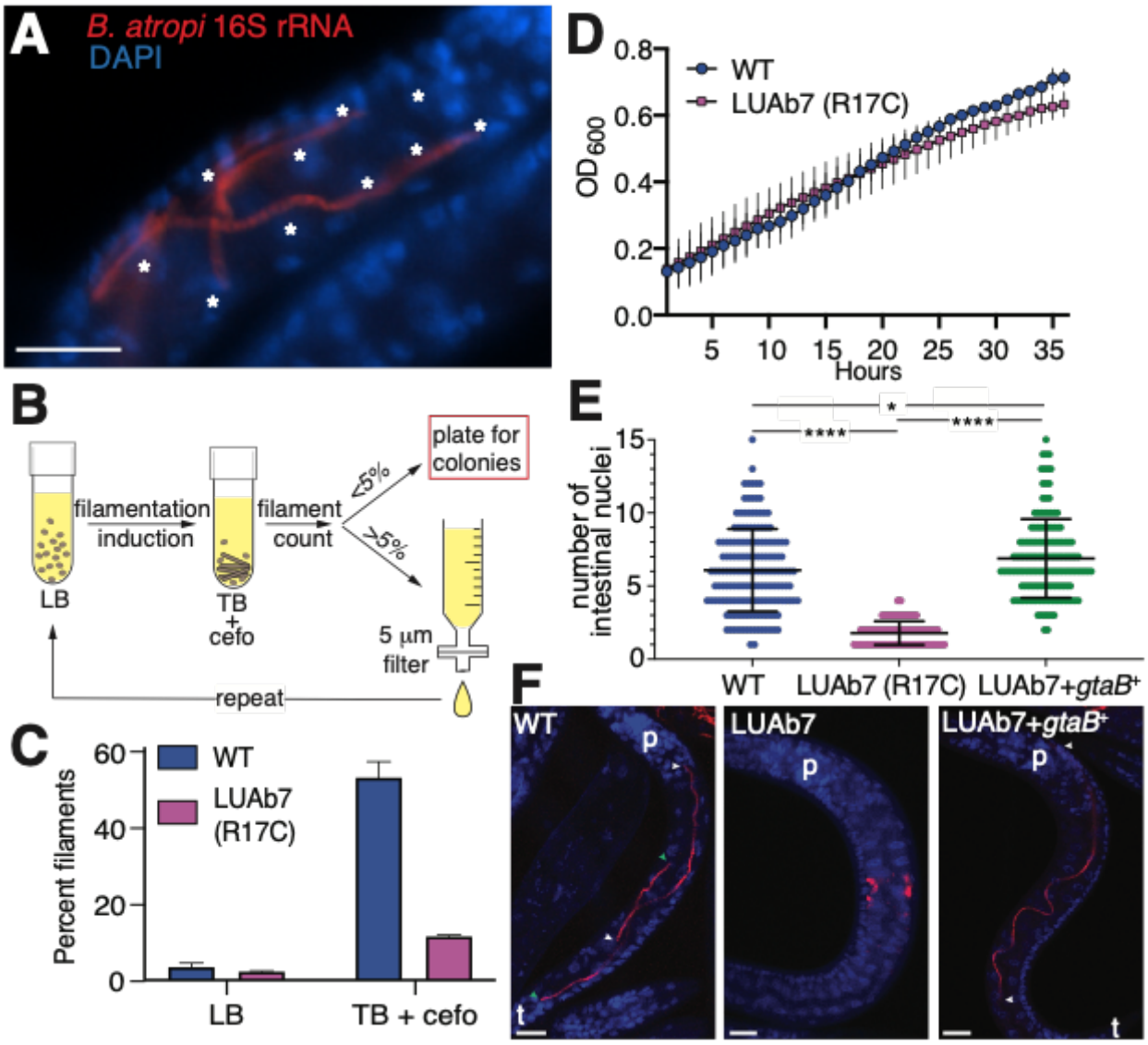

Fig. 2. *B. atropi* filaments invade multiple intestinal cells. (**A**) Filaments of *B. atropi* in a larval *O. tipulae* animal with host nuclei indicated (*). (**B**) Schematic for selection of filamentation mutants. Filamentation was induced with TB + cefotaxime and counted for percent population with filaments, with >5% resulting in filtration followed by a repeat of induction and <5% resulting in plating to isolate single colonies. (**C**) Growth of *B. atropi* in LB or TB + cefotaxime, with percent filaments counted after 48 hours at 32°C. (**D**) *B. atropi* strains grown in LB at 32°C for 36 hours with OD_{600} taken every hour. (**E**) Quantification of *B. atropi* infection in vivo by the number of intestinal nuclei that a single filament or contiguous infection passes along on the anterior-posterior axis. Results are from 2 independent replicates, n>60 infectious events per replicate, p<0.0001 (****) or p=0.014 (*) by Mann-Whitney two-tail t test. (**F**) Representative images from (E), with filament ends (*color-matched arrowheads*), the pharynx (*p*) and tail (*t*) indicated. Scale bars are 10 µm.

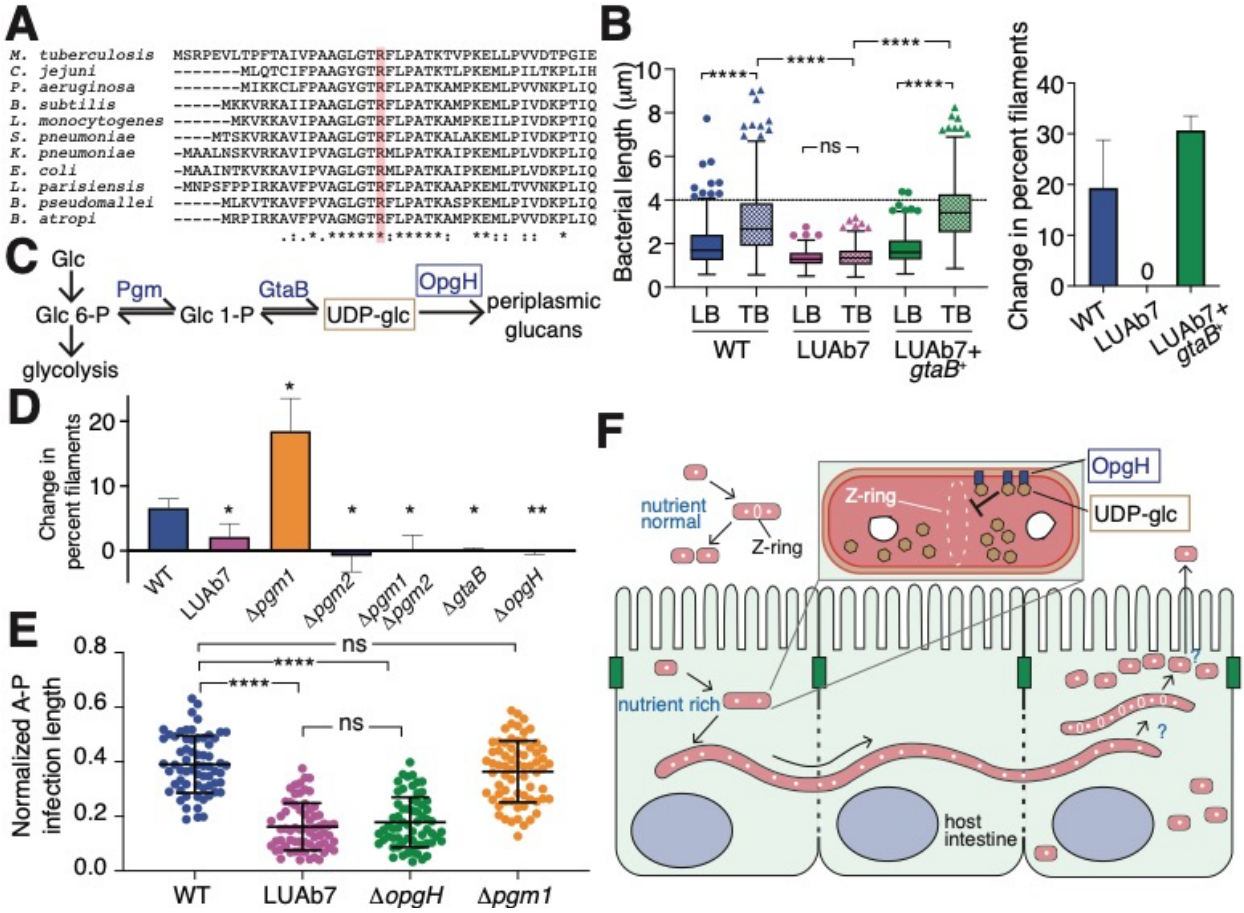

Fig. 3. The role of the UDP-glucose biosynthetic pathway in filamentation. (**A**) CLUSTAL O multiple sequence alignment of GtaB from divergent bacteria with the predicted catalytic arginine highlighted. (**B**) In vitro filamentation of LUAb7(*gtaB*^{R17C}) and the complemented LUAb7 + *gtaB*$^{+}$ as measured by bacterial length in LB and TB (n=150, 2 independent replicates, Tukey's plot). The cutoff for a filament is 4 μm (hatched line) (*left*). The change in percent filaments was measured (% filaments in TB - % filaments in LB) (*right*). (**C**) The UDP-glucose biosynthetic pathway converting glucose (*glc*) to UDP-glucose (*UDP-glc*). (**D**) *B. atropi* knockouts measured for the change in percent filaments. Results are from 3 independent replicates, n>400 bacteria per replicate, $p<0.05$(*) or $p<0.01$(**) by unpaired two-tail t test with Welch's correction compared to WT. (**E**) Anterior to posterior (A-P) spreading of *B. atropi* mutants in vivo, normalized to animal length. Results are from 2 independent replicates, n=32-36 animals per replicate, $p<0.0001$ (****) or not significant (*ns*) by Mann-Whitney unpaired two-tail t test. (**F**) Model for *B. atropi* intracellular filamentation and spreading.